LBL-11127

Lawrence Berkeley Laboratory
UNIVERSITY OF CALIFORNIA

Materials & Molecular
Research Division

Submitted for the International Corrosion Forum
Sponsored by the National Association of Corrosion
Engineers, Houston, TX, March 22-26, 1982

# THE EFFECT OF SURFACE DOPING ON THE OXIDATION OF $Cr_2O_3$ - FORMING ALLOYS



M. Landkof, D.H. Boone, D.P. Whittle,
and A.V. Levy

December 1981



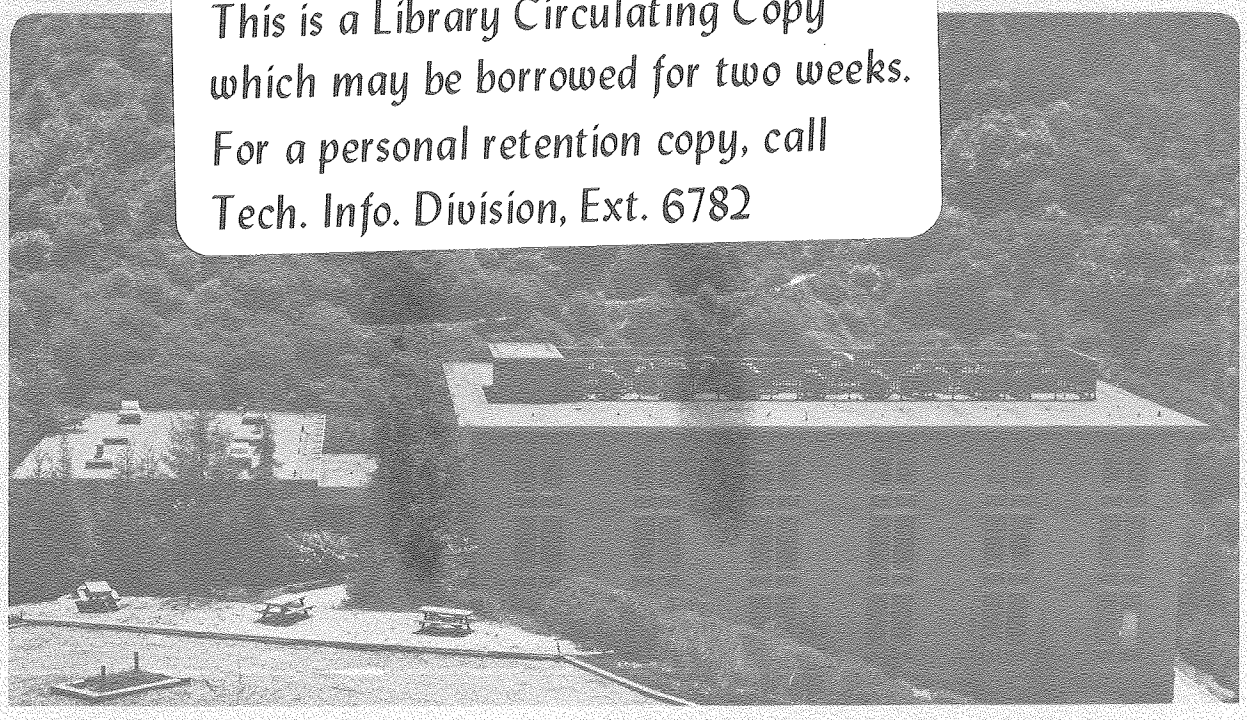

Prepared for the U.S. Department of Energy under Contract W-7405-ENG-48

## DISCLAIMER

# THE EFFECT OF SURFACE DOPING ON THE OXIDATION OF $Cr_2O_3$ - FORMING ALLOYS

M. Landkof, D. H. Boone, D. P. Whittle and
A. V. Levy
Lawrence Berkeley Laboratory
Materials and Molecular Research Division
University of California
Berkeley, California 94702

## Abstract

The influence of the surface application of active elements (doping) on the composition, morphology, adherence and the growth rate of oxide scales formed during high temperature exposure has been investigated. The active elements were applied as an aqueous solution of nitrate salts which were subsequently thermally decomposed to the oxide. Y, Ce, La, Hf, Ca, and Zr were used as the active elements on 304 and 310 stainless steels.

The application of the dopants on the surface was found to enhance the oxidation resistance of the alloy in the case of Y, Ce, La additions while no benefits were found for alloys doped with Hf, Ca and Zr. The possible reasons for these variations in behavior are discussed.

## I. Introduction

The beneficial effects of active element additions (doping) on the oxidation resistance of different heat resistant alloys are well known.[1-10] Among the active elements that have been used are yttrium (Y), cerium (Ce), lanthanium (La), hafnium (Hf), calcium (Ca) and zirconium (Zr). The major improvements observed were better adherence of the protective scale to the substrate, slower rates of overall oxidation (particularly for $Cr_2O_3$ formers), and more rapid establishment of a $Cr_2O_3$ scale in the initial stages of exposure. Although there is no generally accepted theory, some explanations have been offered for these improvements. The oxygen active elements may act as nucleation sites for initial scale formation thus

This work was supported by the Director, Office of Energy Research, Office of Basic Energy Sciences, Materials Sciences Division of the U.S. Department of Energy under Contract Number W-7405-ENG-48.

reducing the distance between the crystal nuclei (often chromia) and shortening the transient stage of oxidation. This also results in a smaller oxide grain size. [8, 9, 10] The better adherence may be caused by lowering the growth stresses as a result of the slower oxidation rate, providing easier accommodation of the growth and thermal stresses because the finer grain size scale is possibly more plastic, or the active element oxides promoting mechanical keying of the scale to the substrate (pegging).[10]

It has also been suggested that the reduction of the oxidation rate of the doped alloys may be a result of the blocking or removing of short circuit diffusion paths (thought to be dislocation networks) for cations.[5] In the extreme case, the oxide forming reaction may move from the oxide-oxygen interface to the oxide - alloy interface, making the slower transport process (inward oxygen diffusion) rate-controlling.[5] This change in mechanism would also decrease or even eliminate void formation at the oxide-alloy interface which would also improve the adherence.

Up to the present, most engineering effort to use this efect has concentrated on internal doping, the active elements being added directly to the alloy or coating as a metal or dispersed oxide. However, one of the original patents[2] suggests direct addition via surface aqueous solution application of a salt of the active element. In addition some attempts at ion implantation of the active element have also been carried out.[11] Recently, unpublished work of Meier et al[12] has described the use of an externally applied slurry of extremely fine oxide powders to modify oxidation behavior of $Cr_2O_3$ forming alloys.

The purpose of this work is to re-examine the possibility of applying the active element via aqueous solution approach since this should provide an inexpensive means of improving the properties of the oxide scale with minimal processing problems and no detrimental effects on the substrate's mechanical properties. A number of different doping elements were tried, all having very high negative free energies for their oxide formation. Two commercial alloys were chosen with different propensities to form a complete chromia layer under normal conditions (high temperature air oxidation without doping). The first, alloy 304 stainless steel (Fe-Cr-Ni), had a borderline Cr content (18%) and does not form a complete external chromia layer without doping. The second alloy, 310 stainless steel, with a higher Cr content (25%) is able to form a complete chromia layer under normal conditions.

## II. Experimental Procedure

The nominal compositions of the alloys used in the investigation are listed in Table I, together with those of the active element nitrates and their source. Coupon specimens, size 15 x 10 x 2 mm, were final polished on a 600 grit SiC paper, ultrasonically cleaned in ethanol and dried. In this study the doping procedure consisted of heating the sample at 500°C in air for 5 minutes and then hot dipping it into a 10% aqueous solution (acidified to approximately pH2) of the active elements' nitrate salt. After drying, the sample was heated for an additional 30 minutes at 500°C to decompose the nitrate salt.

The treated specimens were oxidized in air either isothermally for 50 hr at 1000°C or by thermally cycling them for 20 hr cycles at 1000°C, cooling to room temperature between each cycle. The oxidized specimens were examined using standard metallography techniques, scanning electron microscopy (SEM) and Scanning Auger microscopy(SAM). The oxides that did not spall were stripped off the substrate by dipping in a 10% bromine-methanol solution so that the scale could be isolated from the substrate for analysis. To further aid in the identification of the oxide structures, x-ray diffraction and Raman spectroscopy analysis were performed by Dr. A. Nageberg of the Sandia Livermore Laboratory. More details on the Raman technique are reported elsewhere.[13]

## III. Results

### 1. Active element doping of 304 stainless steel alloy

The samples after isothermal oxidation (50 hr at 1000°C) are shown in Fig. 1. Y, Ce and La doping prevented spalling of the oxide scale. The oxides on the Zr, Hf and Ca doped samples spalled off to about the same degree as occurred on the undoped 304SS sample. The adherent scale formed on the Y, Ce and La doped specimens had a dark blue color on the outer surface and was brown on the under surface.

Cross sections of the Y, Ce and La doped specimens and the undoped 304SS were prepared and studied in the SEM. In Fig. 2 a cross-section of the undoped scale on 304SS in an area where it remained adherent is shown. This scale was ~25μm thick and was primarily iron oxide with some spinel, $FeCr_2O_4$. The Y doped scale on 304SS, Fig. 3, was about 1/5th the thickness of the scale on the undoped specimen and consisted primarily of $Cr_2O_3$ with a small amount of manganese; no iron could be detected using EDAX.

In Fig. 4 the cross section of the Ce doped scale is shown. This scale is thicker than that of the Y doped scale but is still much thinner than that of the undoped 304SS. The scale consisted primarily of $Cr_2O_3$ but some isolated areas rich in iron oxide were detected. The Y, Ce and La doping of the 304SS surface resulted in the formation of more adherent Cr rich oxide scales. The spalled scales of the Hf, Zr and Ca doped specimens were not analyzed in the SEM. However, their color and appearance was so similar to the spalled scale of the undoped 304SS that their structure and composition can be expected to be the same as that observed in Fig. 2 on the undoped alloy.

The unspalled scale on the yttrium doped specimen was stripped off with a 10% bromine-methanol solution and analyzed in the SEM and EDAX. The spalled pieces of the undoped scale were also studied. The outer surface of the doped scale was composed primarily of chromia containing a small amount of manganese (see Fig. 5). On the under surface of the scale, significant amounts of $SiO_2$ in addition to the $Cr_2O_3$ were found. (see Fig. 6). The spalled pieces of oxide from the undoped alloy, shown in Fig. 7, were almost pure iron oxide at the high protrusions on the outer surface with some

Mn (probably in the form of $FeMn_2O_4$) between the protrusions. The inner surface was rich in Cr but with quite high amounts of iron (probably $Cr_2O_3$ + $FeCr_2O_4$), noticeable amounts of chromium (probably $Cr_2O_3$ + $FeCr_2O_4$), noticeable amounts of Si ($SiO_2$) and some Ni ($NiCr_2O_4$). The iron oxides identified by x-ray diffraction were $\alpha$ $Fe_2O_3$ and $\gamma Fe_2O_3$.

The morphology of the outer surface of the yttrium doped oxide scale consists of very small, <5μm, tightly packed crystalites, relatively uniforn in size. See (Fig. 5a). On the inner surface of the Y doped scale, Fig. 6, $SiO_2$ webs can be seen in areas apparently conforming to the underlying alloy grain boundaries. No indication of classical oxide pegs were found in the doped scale to account for the increased scale adherence as occured in some alloys with internally added active elements. Compared to the Y doped scale, the undoped outer surface scale on 304SS is much less-uniform (See Fig. 7a). High protrusions of almost pure iron oxide can be seen. Iron oxide rich layers separated by chromium oxide rich layers could be seen in the cross section (Fig. 2).
Table II summarizes the visual observations and results of the 20 hours at 1000°C thermal cycles .

2. Yttrium doped alloys - oxidation

304SS Alloy

The most pronounced effect of surface active element doping with Y was observed on 304SS alloy. The doping affected the adherence, the thickness, the composition and the morphology of the oxide scale formed. The doped scale did not undergo any spallation after eight 20 hr cycles at 1000°C while the scale on the undoped alloy spalled on the first cycle. The average thickness of the doped scale was about 5μm compared to 25μm for the undoped alloy in areas where part of the scale remained attached to the alloy surface. (See Fig. 2). Some of the spalled pieces from the undoped alloy were even thicker. The results are summerized in Table III.

310 Alloy

The oxide scale formed on the Y doped sample was thinner than the scale on the undoped specimens. (See cross-sections Fig. 8). As shown in Fig. 9 the outer surface of the scale is composed of tightly packed crystallites similar to those seen on the outer surface of the Y doped 304SS scale. On the undoped oxide of the 310SS the $Cr_2O_3$ crystallites are non-uniform in size, see Fig. 10. No noticeable difference could be detected in adherence and the chemical composition of the oxide scale formed on the Y doped and the undoped 310SS specimens. The results are summarized in Table IV.

Active Element Distribution in the Scale

The Scanning Auger microscope (SAM) was used to determine the location of the dopant element, yttrium, during the various stages of nitrate

decomposition and oxidation of 304SS. After the decomposition stage (1/2 hr at 500°C) yttrium could be readily detected in the surface film (see Fig.11). The thin film (~800Å) was mostly $Y_2O_3$ with some chromium and iron oxide formed near the scale-metal interface. After a short oxidation period at high temperature (15 min at 1000°C) the yttrium could barely be detected in the $Cr_2O_3$ scale which formed, Fig 11. A high Cr content found in the scale indicates the presence of $Cr_2O_3$. Some manganese oxide was found in the outer surface of the scale. The 1000°C temperature probably promoted an initial preferential oxidation of Cr and Mn because of enhanced diffusion at the higher temperature. However, the absence of the iron oxides even after longer oxidation times cannot be solely explained by this enhanced diffusion since iron oxides were observed on the undoped 304SS after the long oxidation times. The presence of yttrium must also be playing a critical role in preventing the iron oxide from forming.

## IV. Discussion

### 1. Method of Applying the Doping Element

The purpose of heating the sample before dipping it into the active element nitrate solution was to form a thin oxide scale that improves the wetting properties of the surface and thus produces a more uniform distribution of the nitrate. The application technique seems to influence the protectivity of the doped scale. When the hot sample was dipped in the nitrate solution the change from a greenish to reddish color appeared on the surface after the fourth thermal cycle, (20 hr at 1000°C ), indicating iron diffusion outward. When the sample was painted or dipped after first being allowed to cool, the iron difusion color change occurred earlier, after the second thermal cycle. The reason for better barrier performance in the first case may be in the better incorporation of the doping salts into the initial thin oxide scale. The $Y_2O_3$ layer produced by using the hot-dipping method was found to be twice as thick as that by cold dipping or painting.

The heating stage (30 minutes at 500°C) after application of the salt was to decompose the nitrate salts and, because no nitrogen was detected, it may be assumed that the decomposition was completed. This salt decomposition, if performed simultaneously with the high temperature oxidation (1000°C), could interfere with the oxide nucleation and growth process as nitrogen oxides released may degrade the protective oxide barrier. The depth of yttrium penetration as an oxide in the doped 304SS alloy after the decomposition stage was observed to be 800Å. Decomposition carried out at a lower temperature, 200°C, resulted in the formation of a slightly thinner protective scale during the subsequent 1000°C oxidation.

Although the enhanced protection from a single application of an active element salt occured for only 8 thermal cycles maximum it appeared that the effect may be prolonged by additional applications of the doping element. It was found that by reapplying the yttrium nitrate after the third thermal cycle very slight spallation appeared after 13 thermal cycles.

2. Different Doping Elements on 304SS

Y, Ce and La were found to be very beneficial with the most pronounced effect occuring on the 304SS. The doping affected the formation rate, composition and morphology of the oxide scale and the scale appeared to be much more adherent. The application of Ce and La was slightly less effective than Y. Some iron was found in the Ce and La doped scales. These scales were thicker and spalled sooner during thermal cycling than the scale formed on the Y doped specimens.

The probable explanation for the beneficial effect of Y, Ce and La on the performance of the oxide barrier scales is that they act as nucleation sites which decrease the distance between the more stable chromia forming nuclei during the early stages of oxidation and, thereby, the oxide grain size. The surface is completely covered by the protective chromia layer at an earlier time. The smaller grain size may also improve the adherence of the scale making the scale more deformable during the growing period and during thermal cycling by allowing easier deformation by sliding along grain boundaries.[10]

The slower oxidation rate which results in a thinner oxide scale may be caused by: 1) Preferential $Cr_2O_3$ formation which has a much slower growing rate than the iron oxide, 2) Enhancing the formation of $MnCr_2O_4$ through which the diffusion is slower and 3) Blocking short circuit diffusion paths (diffusion along dislocations). In the most extreme case this may cause a change in the oxide formation mechanism from outward cation diffusion to inward oxygen anion diffusion. Thus, less voids form at the metal-oxide interface that may result in better adherence. [5, 10] This behavior is quite similar to that obtained by interal doping[3-10] of the alloys. Another benefit of external doping is that it does not appear to adversely affect any of the mechanical properties of the alloy as internal doping has sometimes been observed to do.[14]

The poor behavior of Hf and Zr externally doped scales was quite surprising. The absence of an active element effect may possibly be explained by their oxides' anisotropic nature which can be more important for external than for internal doping, especially during the initial stages of oxidation. The thermal expansion along one of their crystallographic axes is extremely low. Also the total polycrystalline thermal expansion of $ZrO_2$and $HfO_2$ in the monoclinic form is somewhat lower than that of the Y, Ce and La oxides, making them more incompatible with higher thermal expansion base metals.

It is well known that some oxides are added to sprayed $ZrO_2$ coatings on metals to stabilize the cubic structure[8] increasing the total linear thermal expansion of the $ZrO_2$. The general spallation of Ca doped samples in the first thermal cycle can be explained by the low melting eutectic that CaO forms, especially with $Cr_2O_3$ (see Table 4) at the test temperature. The closer the working temperature is to the melting point of

the oxide the higher is the possibility of oxygen transfer to the metal-oxide interface.[15] The suggested mechanism for the oxide formation on undoped and doped 304SS, as found in these studies, is summerized in Fig. 12 and 13.

3. Effect of Chromium Content

The 310SS with 25% Cr forms a complete chromia layer more readily than does the 304SS, even without any additives. The active element doping of the 310SS alloy, therefore, did not have as marked an effect on the ability to form a good barrier oxide scale at 1000°C. However, some improvement in the scale morphology and the oxidation rate was still observed. The non-uniform growth of the oxide scale on the undoped sample in comparison to the uniform growth of the scale on the doped sample supports the suggestion that doping elements act as a nucleation site during the initial steps of the oxidation reaction . There still may be some influence of the doping on adherence during thermal cycling. Up to now the tests done on the higher Cr content 310SS were only isothermal. As already indicated in the case of 304SS, the doping strongly affected the oxidation mechanism and seemed to change it entirely. For 310SS the effect was not as marked and there was probably not the major change in the mechanism that occured in the lower chromium content 304SS.

## V. Conclusions

The external surface doping of chromia forming alloys with the active elements Y, Ce and La significantly improved the oxidation resistance of the alloys tested, particularly that of the lower Cr containing 304 stainless steel. The effect of yttrium was the most pronounced. Yttrium seems to slow down the oxidation rate of the 304SS by: (1) causing preferential $Cr_2O_3$ formation which grows much slower than iron oxides, (2) enhancing $MnCr_2O_3$ (spinel) formation through which the diffusion is slower than through pure $Cr_2O_3$ and/or 3) blocking short circuit diffusion paths.

The results of surface doping of the higher Cr alloy, 310SS, strongly supports the suggestion that the main initial effect of the doping is to promote nucleation sites, thereby causing more uniform and smaller oxide scale grain size of the oxide scale to be formed.

The low application cost of external doping using aqueous nitrate salts compared to internal doping (particularly in large and complex engineering shapes) and the absence of apparent detrimental effects of the dopant on mechanical properties of the base alloys are additional advantages of this method of active element addition to enhance the oxidation resistance of elevated temperature service alloys.

In order to better understand the doping mechanism in chromia former alloys it is necessary to carry out external doping experiments using pure alloys with borderline Cr concentrations and without Mn and/or Si.

Acknowledgment

This work was supported by the Director, Office of Energy Research, Office of Basic Energy Sciences, Materials Sciences Division of the U. S. Department of Energy under Contract Number W-7405-ENG-48.

References

1. L. B. Pfeil 1937 U.K. Patent No. 459484

2. L. B. Pfeil 1945 U. K. Patent No. 574088

3. J. M. Francis and W. H. Witlow, Corros. Sci. 5, 701 (1965).

4. G. C. Wood and J. Boustead, Corrs. Sci. 8, 719 (1968).

5. J. Stringer, B. A. Wilcox and R. I. Jaffe, Oxid. Met. 5, 11 (1972)

6. I. G. Wright and B. A. Wilcox. Oxid. Met. 8, 283 (1974).

7. F. A. Golighty, G. H. Stott and G. C. Wood, Oxid. 10, 193 (1976).

8. D. P. Whittle, M. E. El-Dahshan and J. Stringer, Corr. Sci. 17, 879 (1977).

9 I. M. Allam, D. P. Whittle and J. Stringer, Oxid. Met. 13, 381 (1979).

10. D. P. Whittle and J. Stringer, Phil. Trans. R. Soc. Lond. A295, 309 (1979).

11. J. C. Touloukian, R. K. Kerby, R. E. Taylor and T. Y. Lee, Thermophysical Properties of Matter - The TPRC Data Series, Vol. 13 - Thermal Expansion of Metallic Solids.

12. G. H. Meier, G. M. Ecer, and R. B. Singh, The Influence of Superficially Applied oxide Powders on the High Temperature Oxidation Behavior of $Cr_2O_3$ Forming Alloys, presented at TMSAIME Fall Meeting, Pitsburgh, PA, Oct. 1980.

13. R. F. Farrow, A. S. Magelberg, R. E. Benner, and P. L. Mattern, Thin Solid Films. 73, 353 (1980).

14. T. Moroishi, H. Fujikawa and H. Makiura, J. Electrochem. Soc. 126, 2173 (1979).

15. Oxidation of Metals and Alloys, A. S. M. Seminar, October 17 - 18, 1970, Ohio.

TABLE I. Active Elements' nitrates used and Source

| Nitrate | Source |
|---|---|
| $Y(NO_3)_3 \cdot 6H_2O$ | Orion |
| $Ce(NO_3)_3 \cdot 6H_2O$ | " " |
| $La(NO_3)_3 \cdot 6H_2O$ | Ventura Corp. |
| $ZrO(NO_3)_2 \cdot H_2O$ | Noah |
| $Hf(NO_3)_4 \cdot XH_2O$ | " " |
| $Ca(NO_3)_2 \cdot 4H_2O$ | Orion |

Table II. Cycling oxidation (20 hr. cycles at 1000°C) visual observation for undoped and doped 304SS specimen.

| DOPING ELEMENT | CYCLE 1 | CYCLE 2 | CYCLE 3 | CYCLE 4 | CYCLE 5 | CYCLE 6 | CYCLE 7 | CYCLE 8 |
|---|---|---|---|---|---|---|---|---|
| Undoped | General spallation | | | | | | | |
| Hf | General spallation | | | | | | | |
| Ca | General spallation | | | | | | | |
| Zr | Beginning of spallation | General spallation | | | | | | |
| Ce | Very small spots of spallation Greenish gray color | No change | No change | Start of general spallation | Increase in spallation with swollen areas | Further increase in spallation with more swollen areas | | |
| Y | No spallation Greenish gray color | No change | No change | Color change to brownish red. No spallation | No change | No change | More brownish red color | Start of spallation, especially on the specimen edges |
| La | No spallation Greenish gray color | Start of general spallation | | | | | | |

TABLE III. Isothermal oxidation (50 hr at 1000°C) visual observation of doped and undoped 304SS.

| | 304SS, Y Doped | 304SS, Undoped |
|---|---|---|
| Spallation | No spallation | General Spallation |
| Thickness | 2-5μm continuous layer | Varying, up to 40μm |
| Composition | Almost pure $Cr_2O_3$ with some $Mn(MnCr_2O_4)$. $SiO_2$ distribution on the underside along apparent alloy grain boundaries. | Almost pure iron oxide on the outer surface and mixed FeCr oxides $(FeCr)_2O_3$ on the under surface with some Ni and Mn imcorporated |
| Morphology | Uniformaly grown groups of small crystallites. | Non-uniform structure. High protrusions of iron oxide. |

TABLE IV. Isothermal oxidation (50 hrs at 1000°C) visual observations of doped and undoped 310SS

| | 310SS, Doped with Y | 310SS, Undoped |
|---|---|---|
| Spallation | No spallation detected after 50 hr oxidation in air at 1000°C. | No spallation detected after 50 hr oxidation in air at 1000°C. |
| Thickness | Thin scale | Thicker scale, 5-8μm. Examining the surface revealed scale-free areas which probably form during lifting and cracking of the scale. |
| Morphology | uniform growing, small crystallites of uniform size. The small crystals are very tightly packed. | Non-uniform growing crystallites of different sizes. Loosely bonded crystals protruding above the surface. |

Figure Captions

Fig. 1. 304 Stainless Steel alloy samples doped with different active elements and exposed for 50 hr. at 1000°C.

Fig. 2. Metallographic cross section and x-ray maps of the 304SS undoped sample oxidixed for 50 hr. at 1000°C in air.

Fig. 3. Metallographic cross section and x-ray maps of 304SS, yttrium doped sample oxidized for 50 hr at 1000°C in air.

Fig. 4. Metallographic cross section and x-ray map of the 304SS cerium doped sample oxidized for 50 hr at 1000°C in air.

Fig. 5. Outer surface (a) and EDAX analysis (b) of 304SS yttrium doped oxide scale removed from the substrate ( 50 hr at 1000°C air exposure).

Fig. 6. Under surface (a) and Si x-ray map (b) of 304SS yttrium doped oxide scale removed from the substrate (50 hr at 1000°C air exposure).

Fig. 7. Outer (a) and under (b) surface and EDAX analysis of the 304SS undoped spalled oxide scale (50 hr at 1000°C air exposure)

Fig. 8. Metallographic cross-section of the 310SS yttrium doped (a) and undoped (b) samples oxidized for 50 hr at 1000°C in air.

Fig. 9. Outer surface (a) and EDAX analysis (b) of the 310SS yttrium doped oxide scale.

Fig. 10. Outer surface (a) and EDAX analysis (b) of the 310SS undoped oxide scale, stripped from the surface.

Fig. 11. Surface structure of the oxide formed on undoped (a) and Y doped (b) 304SS after 1/2 hr at 500°C air exposure.

Fig. 12. Schematic representation of possible sequence of oxidation events observed during the 1000°C exposure of undoped 304SS.

Fig. 13. Schematic representation of possible sequence of oxidation events observed during 1000°C exposure of Y doped 304SS.

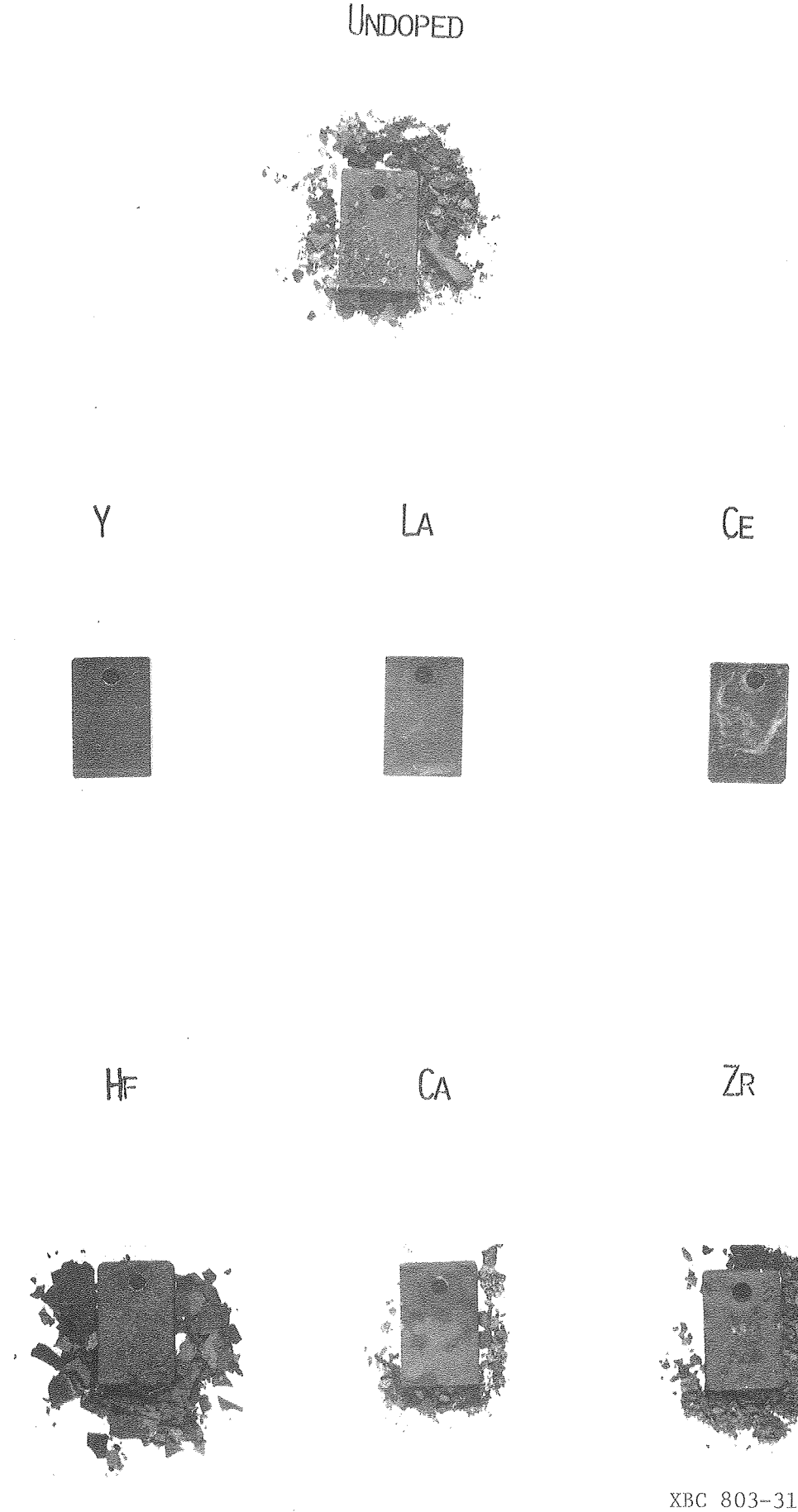


XBC 803-3113

**FIG. 1 304 STAINLESS STEEL ALLOY**

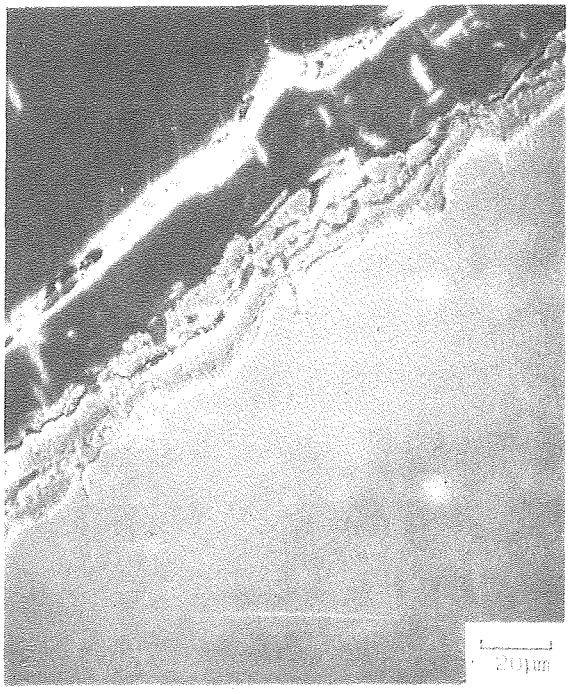


Cr Map

Fe Map

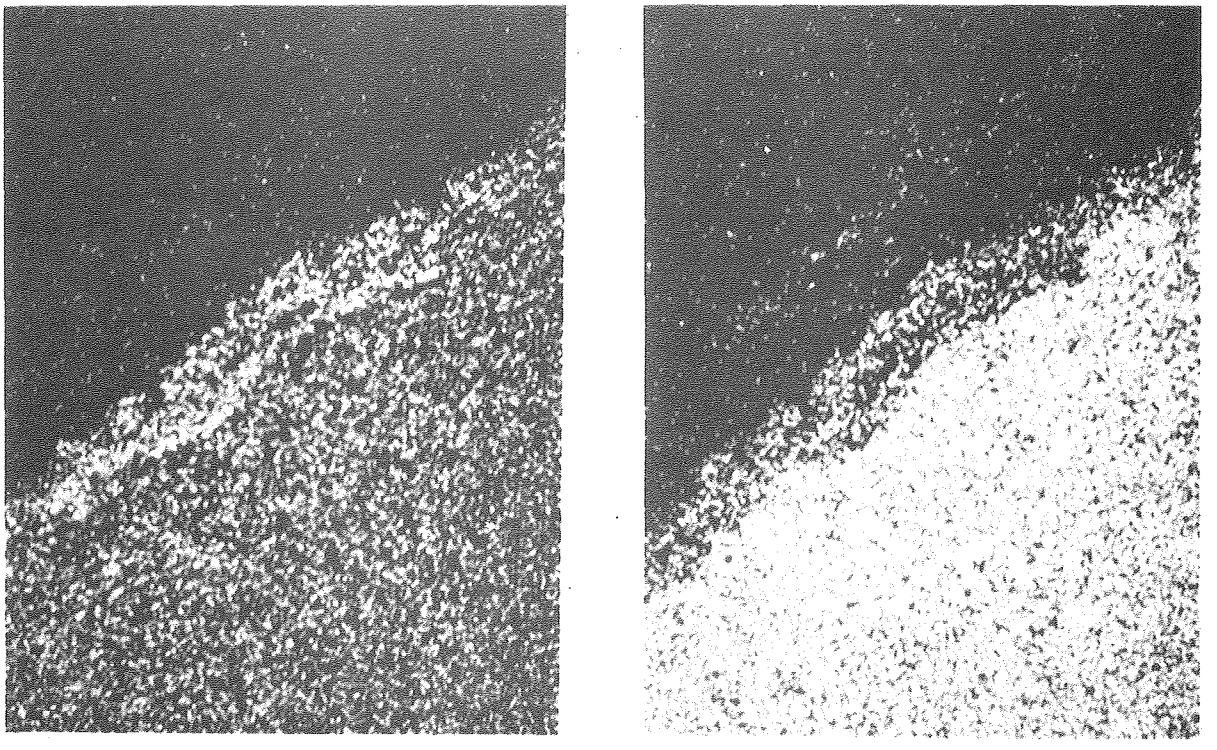

XBB 805-6208

Fig. 7 Undoped Sample of 304 SS


Cr Map

Fe Map

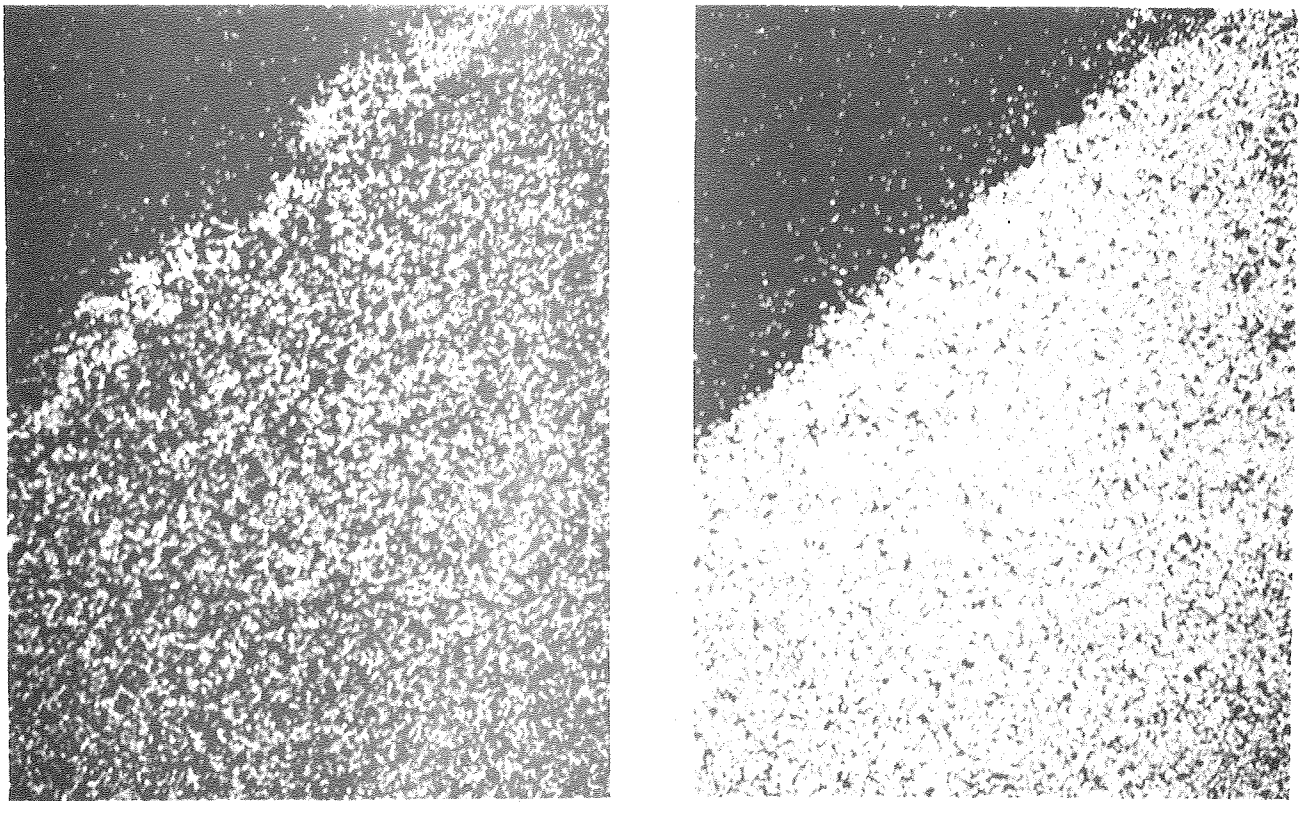

XBB 805-6209

Fig. 3 Yttrium Doped 304 SS Sample

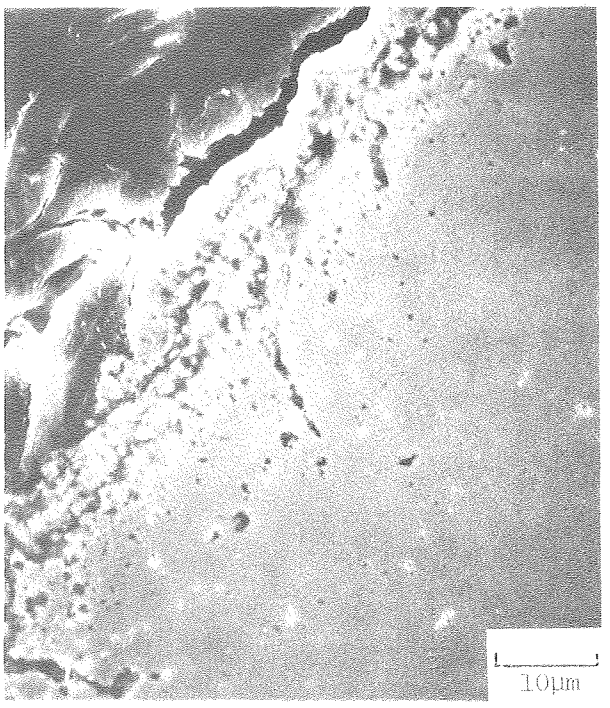


Cr Map

Fe Map

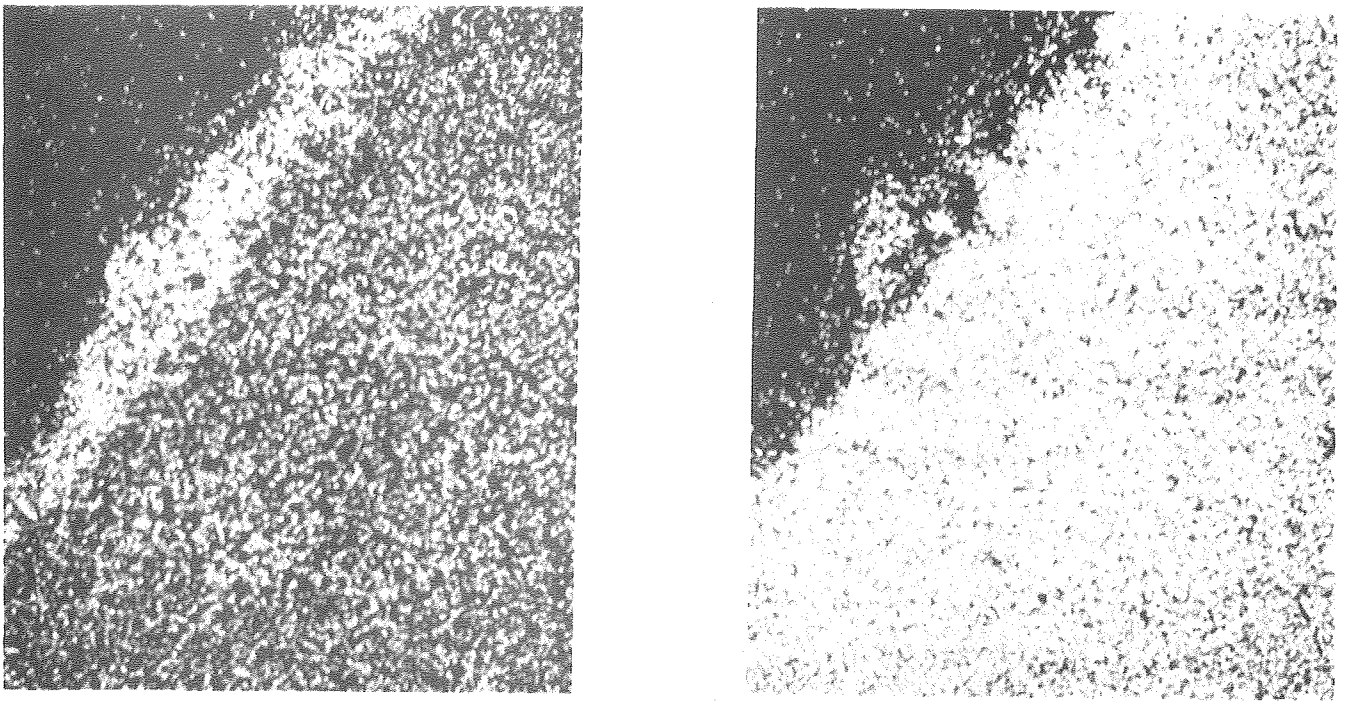

XBB 805-6210

Fig. 4 Ce Doped 304 SS Sample

a

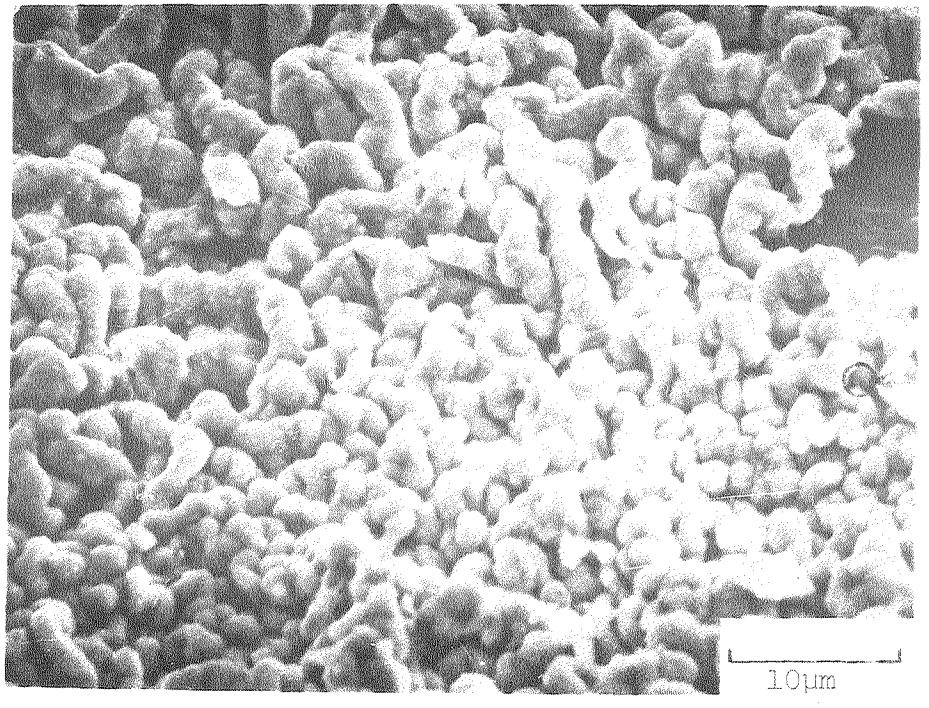


b

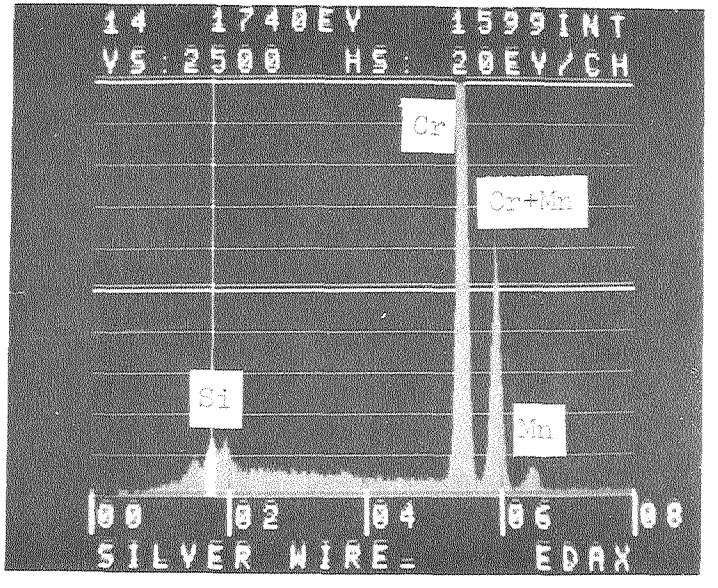


XBB 805-6200

Fig. 5 304 Stainless Steel Y Doped - Outer Surface

a

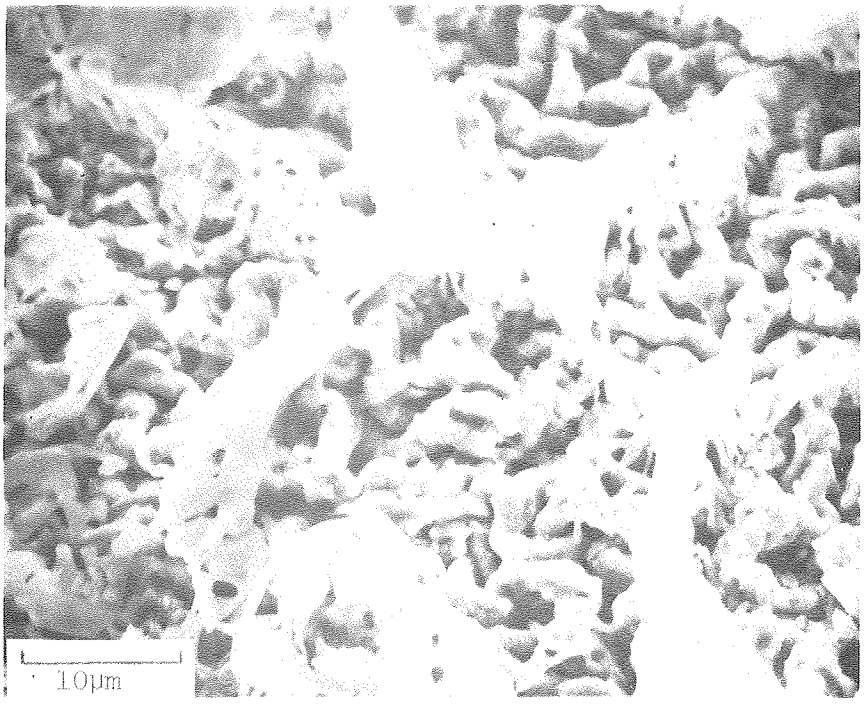


b

Si Map

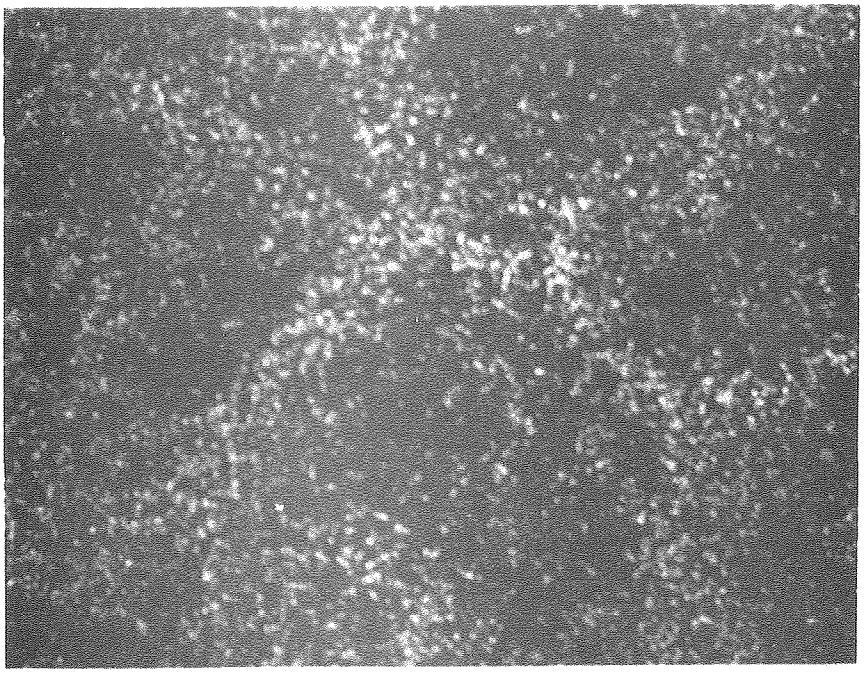

XBB 805-6205A

304 Stainless Steel Y Doped - Under Surface

Fig. 6

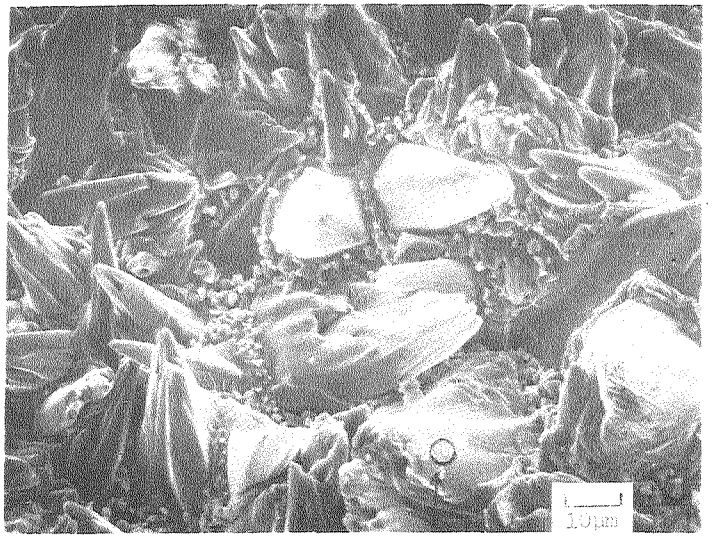

Outer Surface

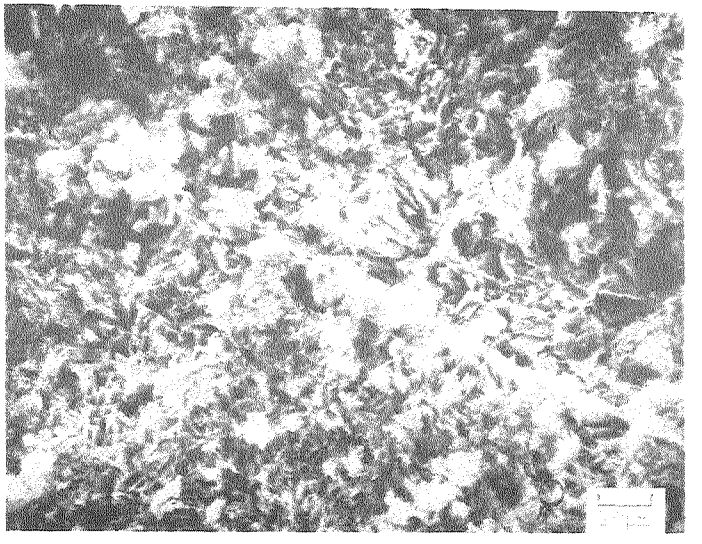

Under Surface

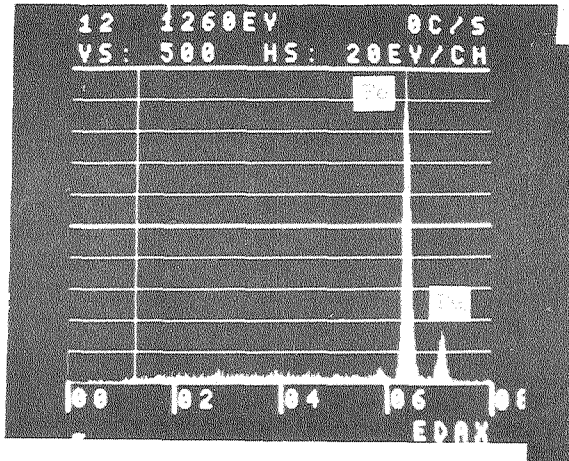


Outer Surface Protrusion

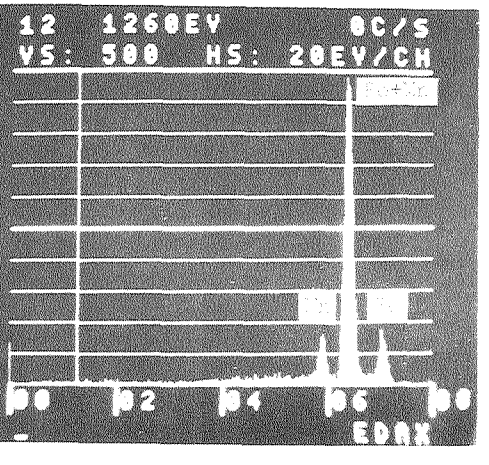


Outer Surface Matrix

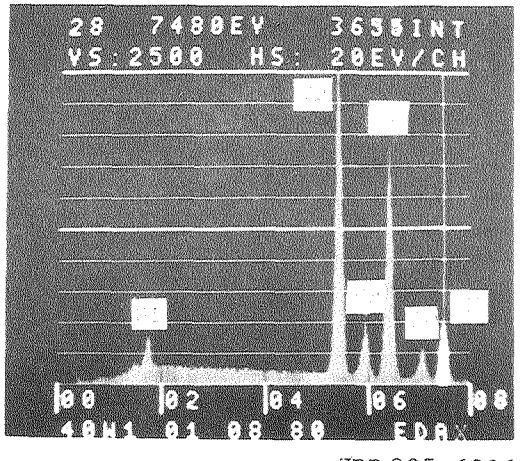


KBB 805-6206

Under Surface

a

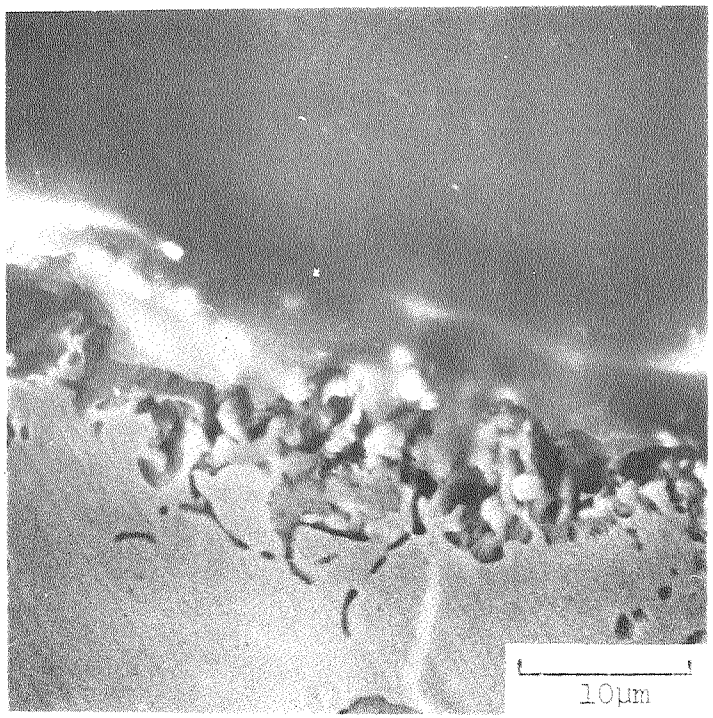


Doped with Y

b

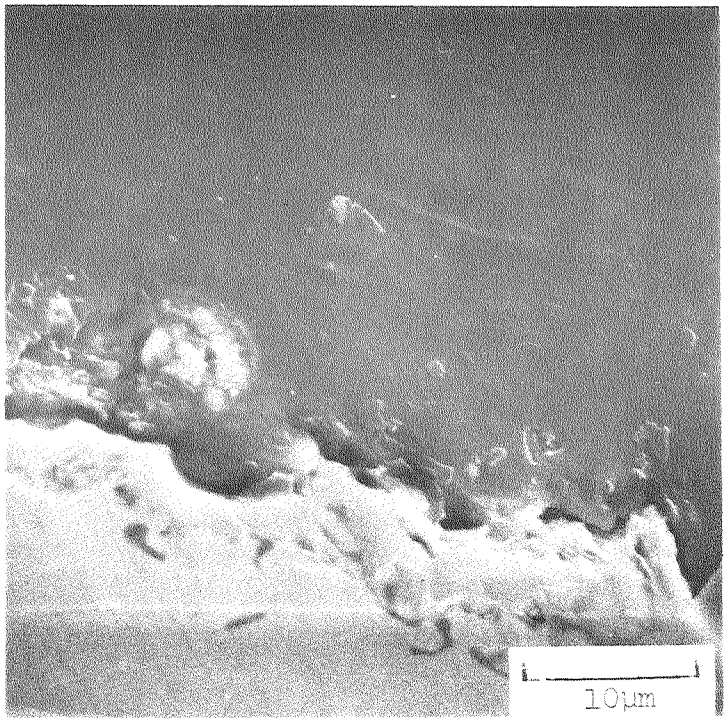


XBB 805-6201

Undoped

Fig. 8 310 Stainless Steel Alloy

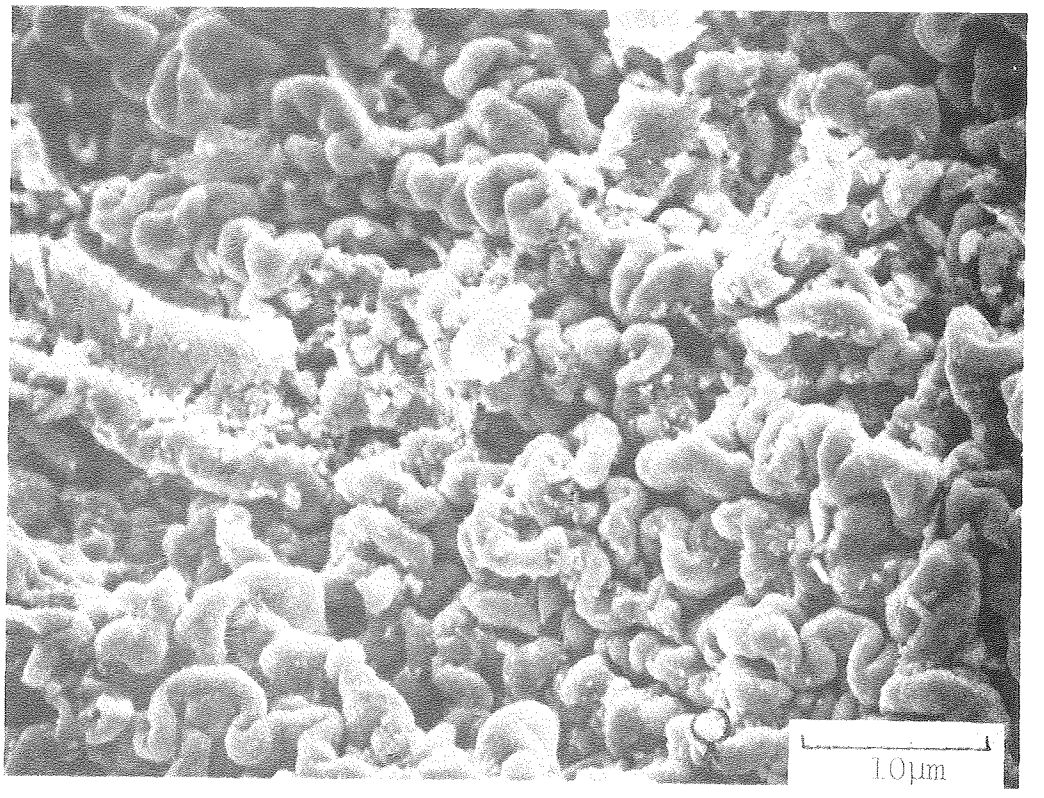


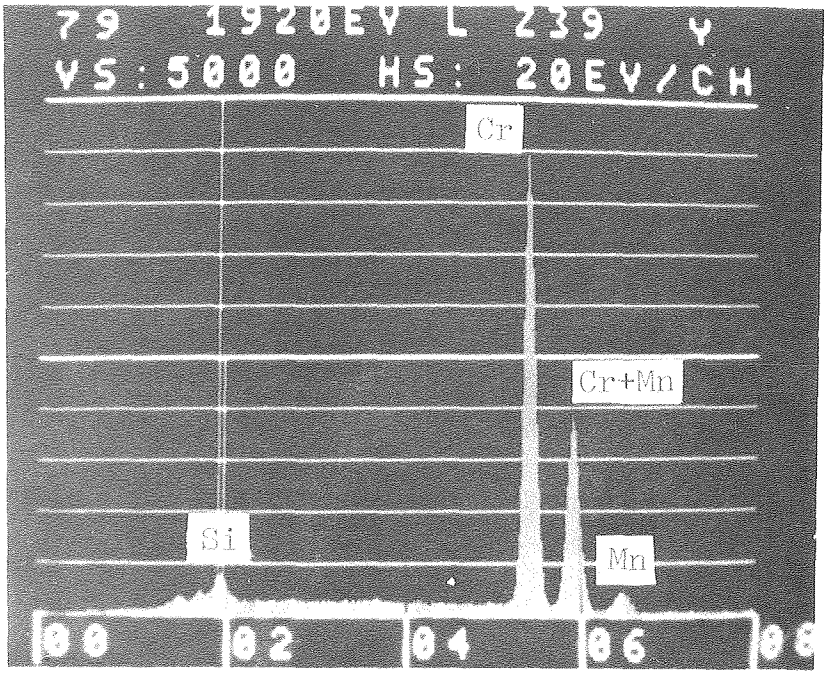


XBB 805-6203

Fig. 9 310 Stainless Steel Y Doped - Outer Surface

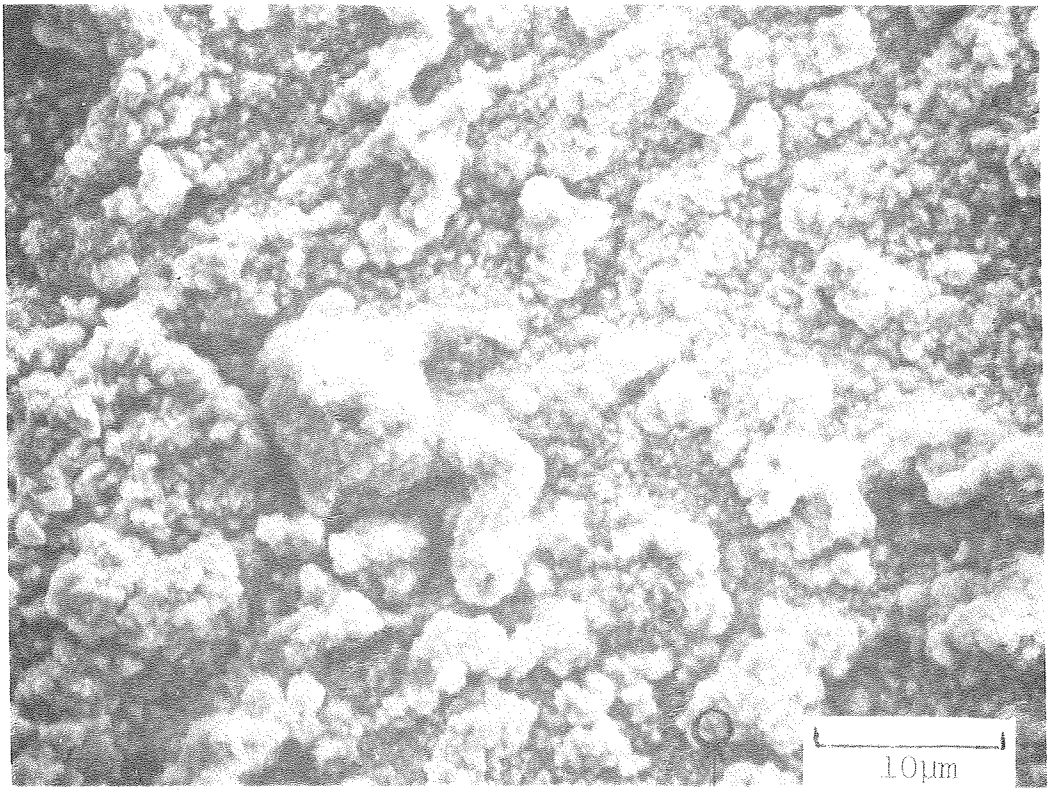


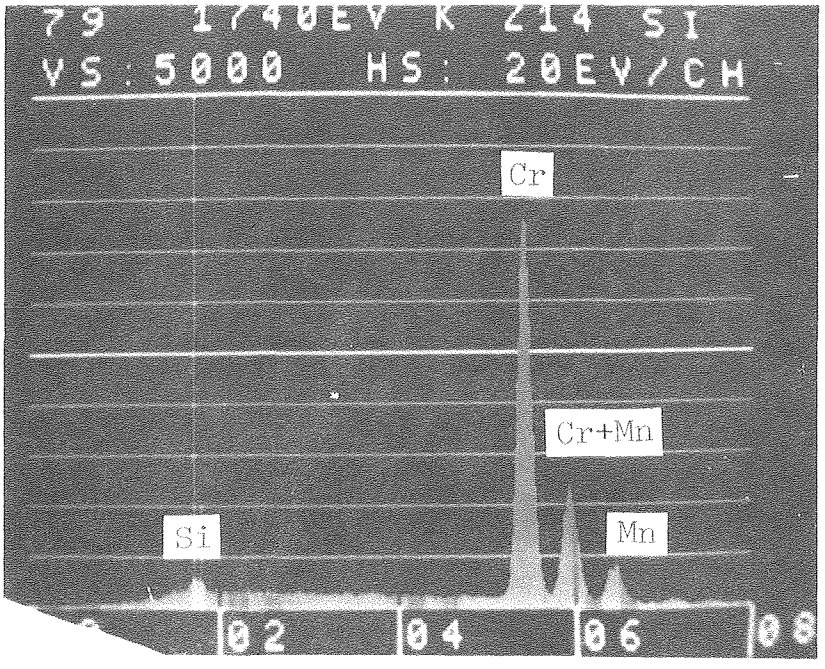


XBB 805-6204

Fig. 10 310 Stainless Steel Undoped - Outer Surface

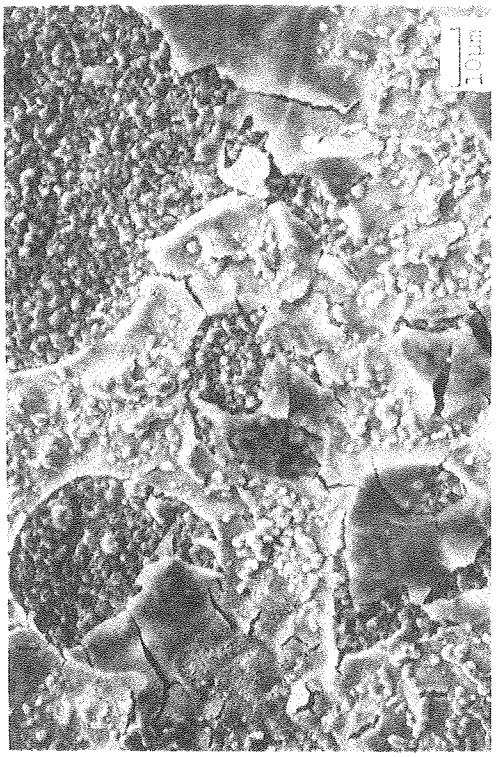


Doped Sample

XBB 805-6207

Doped Sample

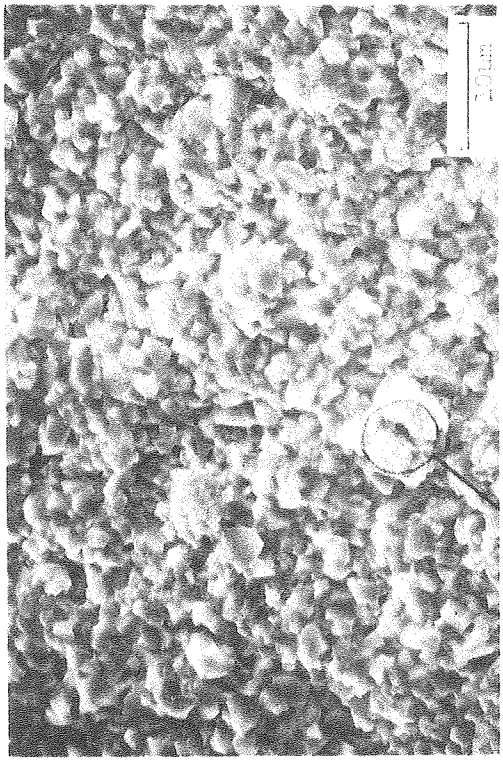


A Undoped Sample

Fig. 11

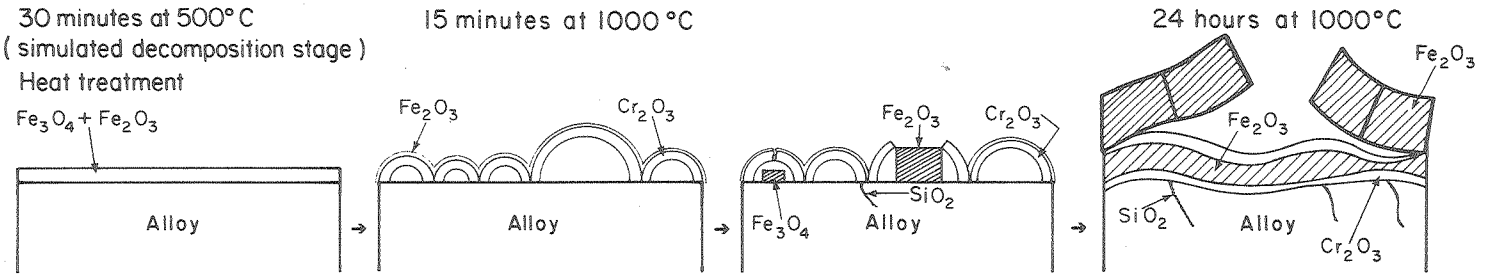


Undoped 304 stainless steel

XBL 809 - 1889

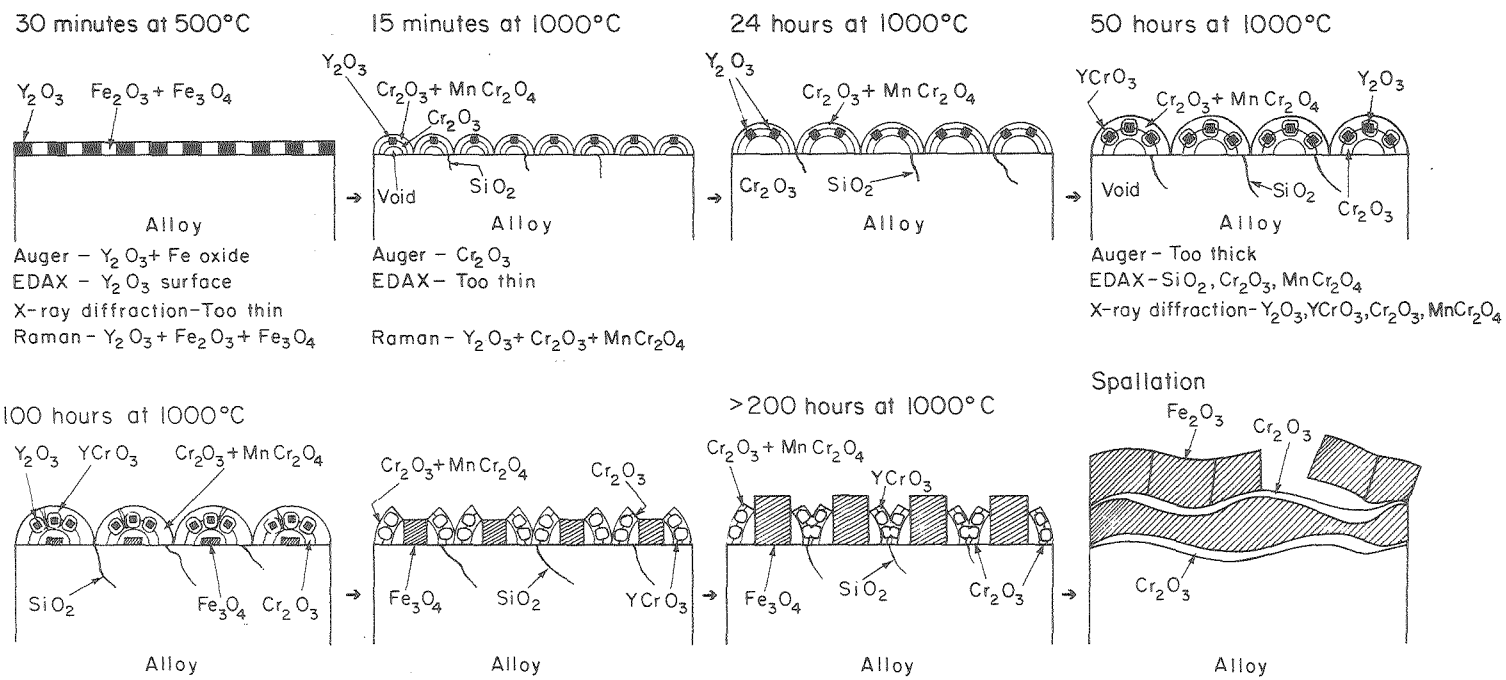


Y-doped 304 stainless steel

XBL809-1890

TECHNICAL INFORMATION DEPARTMENT
LAWRENCE BERKELEY LABORATORY
UNIVERSITY OF CALIFORNIA
BERKELEY, CALIFORNIA 94720